Cell Reports
Resource

An In Vivo Functional Screen Uncovers miR-150-Mediated Regulation of Hematopoietic Injury Response

Brian D. Adams,[1] Shangqin Guo,[1] Haitao Bai,[1,5] Yanwen Guo,[1] Cynthia M. Megyola,[1] Jijun Cheng,[1] Kartoosh Heydari,[2] Changchun Xiao,[3] E. Premkumar Reddy,[4] and Jun Lu[1,*]
[1]Department of Genetics, Yale Stem Cell Center, Yale Cancer Center and Yale Center for RNA Science and Medicine
[2]Department of Immunobiology, Yale Flow Cytometry Core Facility
Yale University, New Haven, CT 06520, USA
[3]Department of Immunology and Microbial Science, The Scripps Research Institute, La Jolla, CA 92037, USA
[4]Department of Oncological Sciences, Mount Sinai School of Medicine, New York, NY 10029, USA
[5]Department of Hematology, Shanghai Jiaotong University Affiliated Shanghai First People's Hospital, Shanghai 200080, China
*Correspondence: jun.lu@yale.edu
http://dx.doi.org/10.1016/j.celrep.2012.09.014

SUMMARY

Hematopoietic stem and progenitor cells are often undesired targets of chemotherapies, leading to hematopoietic suppression requiring careful clinical management. Whether microRNAs control hematopoietic injury response is largely unknown. We report an in vivo gain-of-function screen and the identification of miR-150 as an inhibitor of hematopoietic recovery upon 5-fluorouracil-induced injury. Utilizing a bone marrow transplant model with a barcoded microRNA library, we screened for barcode abundance in peripheral blood of recipient mice before and after 5-fluorouracil treatment. Overexpression of screen-candidate miR-150 resulted in significantly slowed recovery rates across major blood lineages, with associated impairment of bone marrow clonogenic potential. Conversely, platelets and myeloid cells from miR-150 null marrow recovered faster after 5-fluorouracil treatment. Heterozygous knockout of *c-myb*, a conserved target of miR-150, partially phenocopied miR-150-forced expression. Our data highlight the role of microRNAs in controlling hematopoietic injury response and demonstrate the power of in vivo functional screens for studying microRNAs in normal tissue physiology.

INTRODUCTION

Tissue stem and progenitor cells, such as hematopoietic stem and progenitor cells (HSPCs), are responsible for sustaining tissue homeostasis and replenishing the loss of mature lineages after tissue injury. A major cause of hematopoietic injury stems from side effects associated with chemotherapy for solid tumors, which often indiscriminately kill or impair the function of HSPCs, leading to bone marrow toxicity with an acute reduction in peripheral blood cell counts (Wang et al., 2006). The affected cell types include platelets and myeloid cells, which are responsible for blood coagulation and controlling infection, respectively. Such undesired side effects can lead to life-threatening conditions in the weeks during and following administration of chemotherapy and often limit therapeutic doses (Wang et al., 2006; Lyman et al., 2003). Thus, understanding the molecular mechanisms governing the recovery rate of circulating mature blood cells remains an important question.

MicroRNA (miRNA)-mediated posttranscriptional control has emerged as a critical regulatory mechanism in diverse biological processes. These small noncoding RNAs target endogenous messenger RNAs, largely through cognitive sites in the 3′ untranslated regions (UTRs), resulting in target degradation or translational inhibition (Bartel, 2009). Multiple laboratories, including ours, have reported that specific miRNAs can control hematopoiesis (Baltimore et al., 2008; Guo et al., 2010; Lu et al., 2008; Garzon and Croce, 2008), yet it remains largely unknown whether miRNAs can regulate hematopoietic recovery rate after injury.

Functional screens can provide a direct and powerful approach to identify gene functions in mammalian biology. Indeed, in vitro screens based on miRNA expression libraries have proven highly useful (Voorhoeve et al., 2006; Izumiya et al., 2010; Huang et al., 2008; Poell et al., 2011). For instance, miR-372/miR-373 were found to be potent oncogenes that have a stronger effect than p53 knockdown in relieving oncogene-induced senescence (Voorhoeve et al., 2006). Despite the successes of in vitro miRNA screens, in vivo miRNA screens have not been reported in mammals. Specifically, questions regarding physiological processes, such as studying HSPCs, are often difficult to model in vitro because hematopoietic stem cells easily lose stemness outside the host environment. Thus, genetic screens to study HSPCs were rarely attempted in vitro or in vivo, often requiring large cohorts of mice (Ali et al., 2009; Deneault et al., 2009; Hope et al., 2010; Wang et al., 2012). Recent studies with barcoded shRNA libraries (Zender et al., 2008; Bric et al., 2009; Meacham et al., 2009; Wang et al., 2012) suggest the prospect of an in vivo barcoded miRNA screen

to study HSPC physiology, with multiple miRNAs screened in each individual mouse, and analysis of barcode abundance to deconvolute the contribution of each miRNA. There are, however, two limiting factors for a barcoded HSPC screen. One is the limited number of HSPCs from in vivo sources, making it challenging to obtain enough cell coverage for large numbers of genetic constructs. Second, only a limited number of normal HSPCs may engraft each lethally irradiated transplantation recipient (Lu et al., 2011), creating a bottleneck for analyzing a large number of genes per recipient mouse. In this regard, miRNAs are especially favorable candidates for medium-sized library screens because only a few hundred miRNAs are predicted to target >30% of the protein-coding transcriptome (Bartel, 2009), thus allowing for a small number of miRNAs to represent substantial gene regulatory perturbations.

In this study, we established an unbiased, in vivo, gain-of-function screen to identify miRNAs involved in modulating hematopoietic recovery in mice upon chemotherapeutic challenge. The term "hematopoietic recovery" in this paper is used to describe the recovery of peripheral blood cells after chemotherapy-induced suppression of peripheral blood parameters, thus reflecting underlying mechanisms of both regeneration and apoptosis of bone marrow progenitors. We modeled chemotherapy response using 5-fluorouracil (5-FU), a clinically used drug for solid cancers (Longley et al., 2003). With a library of 135 hematopoietic-expressed miRNAs, we assayed the function of 35–71 miRNAs in each recipient mouse. Three out of four screen candidates were validated to inhibit hematopoietic recovery. Among them, gain- and loss-of-function experiments established the importance of miR-150, partially through targeting *c-myb*, a conserved miR-150 target. Our data highlight the role of miRNAs in controlling response of HSPCs toward tissue injury and demonstrate the feasibility and power of functional in vivo barcode screens for studying tissue physiology.

RESULTS

Injury from 5-FU Induces Vast miRNA Expression Changes in the Bone Marrow

To identify miRNAs that regulate hematopoietic response after 5-FU-induced injury, we initially analyzed miRNA expression changes in bone marrow cells from mice with or without 5-FU treatment. Global miRNA expression profiling of the 5-FU and untreated cohorts showed that 92 miRNAs (among 168 that passed the detection threshold) were significantly upregulated or downregulated, with false discovery rates <5% (Figure S1A; Table S1). This large number of altered miRNAs made it difficult to identify which miRNAs serve as functional regulators of hematopoietic injury response. We thus went on to perform an in vivo functional screen.

Developing a miRNA Expression Library and Bead-Based Barcode Detection System

As a first step toward establishing a physiologically relevant in vivo gain-of-function screen, we constructed an expression library comprised of individual miRNAs that are expressed in the hematopoietic system (Figure S1B). These miRNAs (Table S2) were chosen from publicly available deep-sequencing data of hematopoietic tissues (Landgraf et al., 2007), largely based on their abundance. In anticipation of limited numbers of HSPCs that may engraft in each mouse (Lu et al., 2011), we restricted the size of the library to 135 miRNAs. For those miRNAs that can be produced from multiple loci in the genome, only a single representative locus was picked. With these design principles, we PCR amplified genomic regions harboring the miRNA hairpins and flanking sequences and individually cloned them into a pMSCV-based retroviral vector, which is widely used to support overexpression in the hematopoietic system (Lu et al., 2008; Guo et al., 2010).

With a miRNA expression library in hand, we then developed an inexpensive bead-based system that can readout the contribution of each library construct among a pool of library-transduced cells (Figure S1C). We took advantage of unique sequences (referred to as barcodes below) present in the hairpin-flanking regions of miRNA-coding genes. Complementary oligonucleotides to barcode sequences were coupled to polystyrene beads embedded with unique combinations of fluorophores. Genomic DNA samples from library-transduced cells could be PCR amplified with biotinylated primers specific to the expression vector, hybridized to the barcode-detector-coupled beads, and labeled with streptavidin-phycoerythrin. A flow cytometer was then used to report the identity of the beads and quantify the barcode abundance detected on each bead.

This bead-based detection system has the specificity and reproducibility required for robust barcode quantification of the miRNA library. To test detection specificity, genomic DNA from miR-29a-transduced HL-60 cells was assayed, and signal was only observed from the respective miR-29a detector (Figure S1D). We next pooled the 135 library constructs, produced virus, and transduced HL-60 cells. The majority of barcodes (130 out of 135, or 96%) could be robustly detected above background (Figure S1D). Independent PCR amplifications from the same genomic DNA sample produced low variance in signals, indicating that the detection system is reproducible (Figure S1E). Thus, with the availability of the expression library and a reliable barcode detection system, we proceeded to the in vivo screen.

An In Vivo Gain-of-Function Screen Reveals Candidate miRNAs Involved in Regulating Hematopoietic Recovery

To uncover miRNA-mediated regulation of hematopoietic injury response upon 5-FU treatment, we performed an in vivo functional screen as illustrated in Figure 1. Adult murine donor bone marrow cells were transduced with the miRNA expression library as a pool and transplanted into lethally irradiated recipient mice. To ensure that donor cells contained largely single copy integrations of the viral constructs, we titered the miRNA library to a transduction efficiency of ~10%–25%. After transplantation, we harvested peripheral blood of recipients at defined intervals, both to monitor the level of engraftment and to prepare genomic DNA for barcode detection. Once engraftment reached relatively stable levels at 11 weeks posttransplantation (Figures S2A and S2B), the recipient animals were treated with 5-FU. Day 10 post-5-FU reflected the time point with strong hematopoietic suppression, whereas day 22 represented normalization of the blood parameters (Figure S2C). We reasoned that miRNAs with barcode signals decreased after 5-FU treatment would suggest

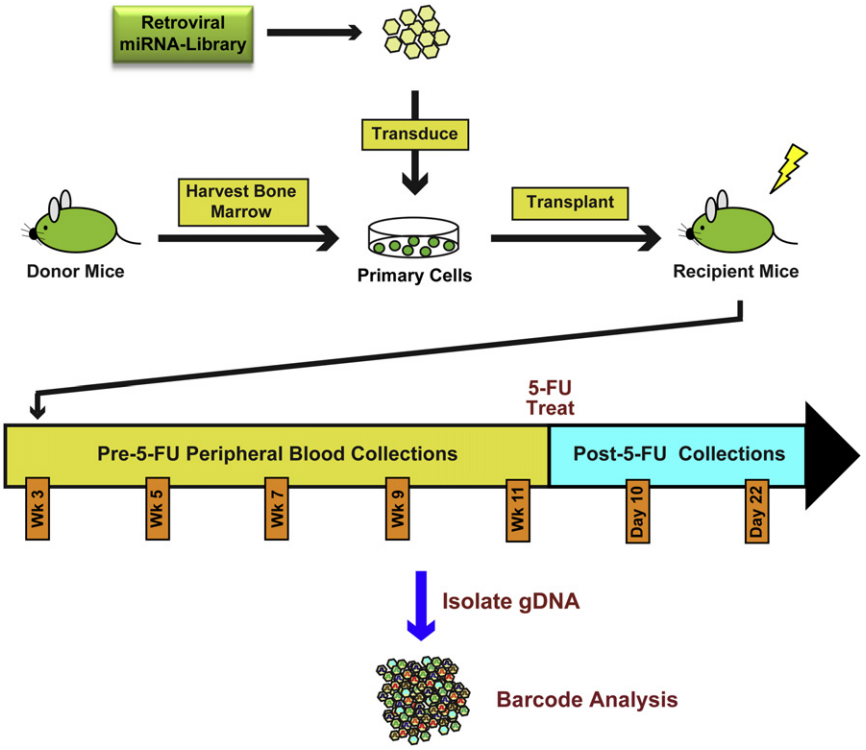

Figure 1. Schematic of the In Vivo miRNA Screen

Donor bone marrow cells were transduced with a pooled miRNA expression library and transplanted into lethally irradiated recipient mice. Peripheral blood samples were collected at indicated weeks (Wk) posttransplantation. Mice were challenged with 5-FU 3 days after the week 11 collection and sampled at indicated days post-5-FU. Genomic DNA (gDNA) was isolated from peripheral blood and subjected to barcode analysis. See also Figure S1 and Tables S2 and S5.

an inhibitory role upon 5-FU-induced hematopoietic recovery, whereas those that increased would be potential enhancers of this process.

A key consideration for the screen is the functional heterogeneity of HSPCs. Some dominant HSPC clones may have a stronger contribution to peripheral blood than other clones. Thus, miRNAs landing in such clones could be misclassified as enhancers of recovery, even though they do not function in this capacity. Conversely, miRNAs integrating into weak HSPC clones could be misclassified as inhibitors. To avoid HSPC heterogeneity confounding interpretation of barcode results, we used a short duration of viral transduction to minimize proliferation of HSPCs during ex vivo culture, thus reducing the likelihood that descendants of the same HSPC clone could be transplanted into different animals. We also performed three independent viral transductions and transplanted into a total of 15 mice, further reducing the possibility of dominant HSPC clones rendering false-positive results in multiple recipients.

Quantification of barcodes revealed several interesting features from this screen:

(1) Barcode signals could be reliably detected from peripheral blood collections of recipient animals, above detection background (Figures S3A–S3C).

(2) On average, the effect of 52 different miRNAs could be assayed in each recipient mouse. At 3 weeks posttransplantation, each recipient contained 62–108 detectable barcodes. This number decreased with time and was largely stabilized by week 11 posttransplantation to 35–71 detectable barcodes in each animal (Figure 2A). This drop in barcode number is likely due to preferential retroviral transduction of transiently amplifying progenitors that only support short-term contribution to peripheral blood, whereas contribution from the less-transduced but more primitive HSPCs supports longer-term engraftment. Constitutive expression of miRNAs that antagonize engraftment may also contribute to this reduction in barcode number.

(3) Barcode patterns differ between mice. Unsupervised clustering of barcode abundance showed that after 3 weeks posttransplantation, there were more differences in barcode patterns between mice than across different time points within the same mouse (Figure 2C). This result suggests that different sets of miRNAs were transduced in different mice and indicates that barcode abundance changes should only be compared within the same recipient across time points.

(4) A large number of barcodes could be collectively detected within the entire screen cohort. At week 3 posttransplantation, 124 barcodes out of 135 (92%) could be detected in at least one recipient, and 115 barcodes (85%) could be detected in at least five different recipients (Figure S3D). At the time points specifically associated with the 5-FU assay (week 11 and 10 days post-5FU), 124 barcodes (92%) could be detected in at least in one mouse, whereas 88 barcodes (65%) were present in at least five mice (Figure 2B). Taken together, the above-mentioned data indicate that it is possible to use a small number of animals to quantify the effects of a moderate number of genes.

To assess the effect of miRNAs during hematopoietic injury response to 5-FU administration, we considered the effect of HSPC heterogeneity and reasoned that miRNA barcodes that showed consistent changes in multiple animals were more likely true candidates rather than false positives. To reflect this concept, we used a consistency score to quantify the barcode abundance changes in the screen cohort (see Experimental Procedures). After comparing day 10 and day 22 post-5-FU time points with the closest pre-5-FU time point (week 11), we assigned downregulation of barcode signals in each mouse

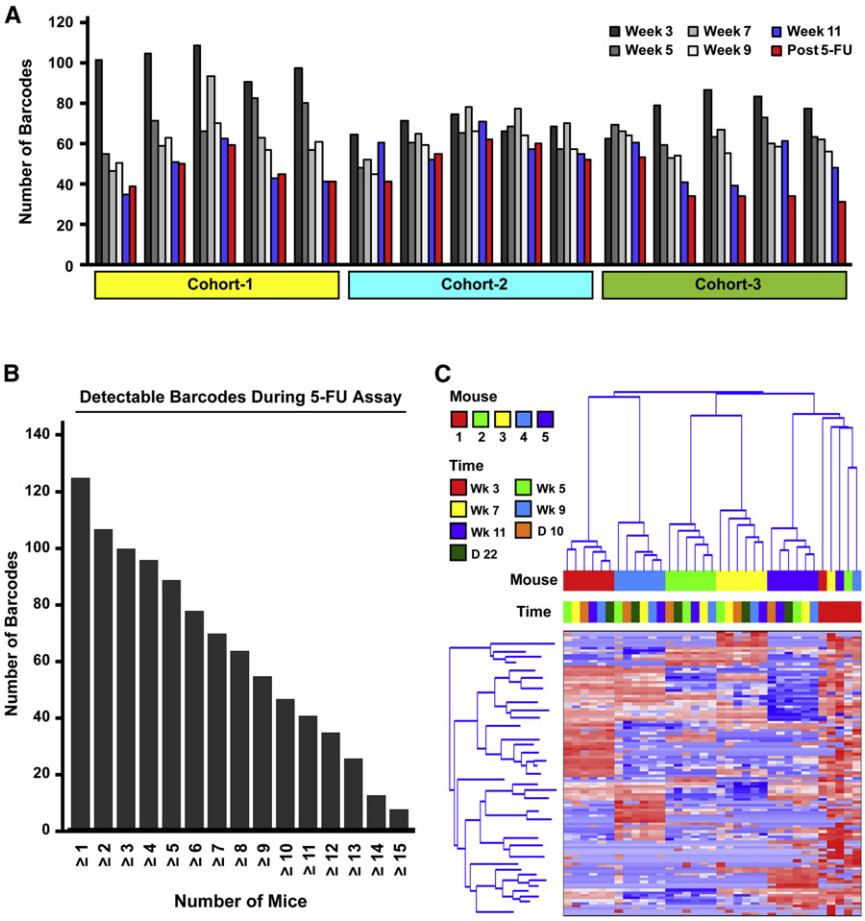

Figure 2. Barcode Analysis from the In Vivo Screen

(A) Barcodes were measured from red cell-lysed peripheral blood samples (effectively from all nucleated cells). The number of barcodes detected in each mouse at different time points is shown. Data were grouped by individual mice from a total of three independent cohorts of 15 mice.

(B) The number of unique barcodes detected in the screen cohort is shown for week 11 post-transplantation and day 10 post-5-FU. Data represent the number of barcodes that can be detected in at least the specified number of mice.

(C) Unsupervised clustering of barcode intensity primarily groups samples by recipient mice. A representative heatmap is shown in which log2-transformed data from samples collected at indicated weeks posttransplantation and days (D) post-5-FU were analyzed. Blue indicates lower signal, whereas red indicates higher signal.

See also Figure S2 and Table S5.

as −1 and upregulation as +1. Thus, miRNAs that antagonized hematopoietic recovery would have a negative consistency score, whereas miRNAs that enhanced recovery would have a positive score. Ranking miRNAs based on these scores, we found that a small number of miRNAs showed consistent trends (Figure 3A), and the rankings were insensitive to variations in analysis parameters (Experimental Procedures; Table S3), indicating minimal analysis artifact.

Upon close inspection, upregulated barcodes showed less consistency, with changes sometimes driven by a single screen cohort. We thus focused on the top four miRNAs whose barcode abundance was decreased in the screen and was distributed across multiple cohorts and across both post-5-FU time points (Table S3; Figures 3A, 3B, and S3E). Thus, miR-153-2, miR-150, miR-301, and miR-652 (ranked from top down) were chosen for further experimental validation.

Forced Expression of miR-150 and Other Candidates Inhibits Hematopoietic Recovery upon 5-FU Treatment

To validate screen candidates, we transduced miR-153-2, miR-150, miR-301, miR-652, or a vector control into donor bone marrow cells and assayed the recovery of these cells in transplant recipients after 5-FU treatment. A constitutive GFP on the vector labeled transduced cells, so competitive recovery of transduced cells versus nontransduced cells within the same recipient mouse could be reflected by GFP^+/GFP^- ratio changes in the peripheral blood. In addition, by using lineage-specific antibodies, we could determine the effects of the miRNA candidates on $Mac1^+$ (CD11b) myeloid cells, $B220^+$ (CD45R) B cells, $CD3^+$ T cells, as well as anuclear CD41+ platelets. For transplant recipients, we followed the GFP^+/GFP^- ratio after transplantation and waited until the ratio largely stabilized before treating mice with 5-FU (Figures S4A and S4B; data not shown). In control recipients, the GFP^+/GFP^- ratio in all examined lineages showed relatively minor perturbations following 5-FU treatment, likely due to mild toxicity of GFP expression (Figure 4). In contrast, the expression of miR-153-2 or miR-150 strongly inhibited both myeloid and platelet recovery (Figures 4A and 4B). Interestingly, expression of the weaker candidate miR-652 led to a weaker yet significant suppression of myeloid and platelet recovery (Figure 4C). Candidate miR-301 did not cause significant changes and is thus a false positive (data not shown). In total, we successfully validated three out of four candidate miRNAs from the screen. Because miR-150 caused a strong inhibitory effect in the validation experiments and is the only miRNA among the three validated candidates that has an available knockout model (Xiao et al., 2007), we thus focused on this miRNA for follow-up experiments.

The miR-150 recipient cohort displayed a significant and sharp decrease in the GFP^+/GFP^- ratio in both myeloid and platelet lineages as early as 7 days post-5-FU (Figure 4A). This strong suppression of the GFP ratio persisted for ~2–3 months and then gradually recovered to levels similar to that of the control cohort. The strongest ratio differential between miR-150 and the control cohort was at 16 days, with platelets suppressed by 4.8-fold and myeloid cells by 2.6-fold. B and

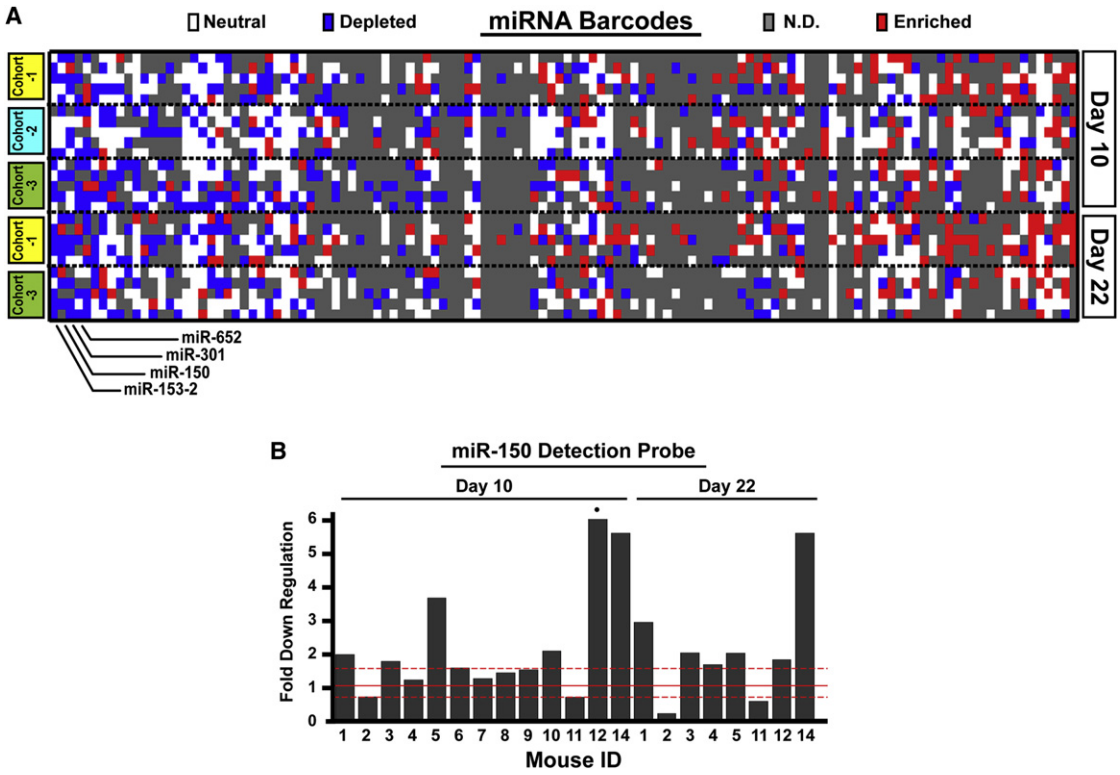

Figure 3. In Vivo Screen Identifies Candidate miRNAs that Inhibit Hematopoietic Recovery

(A) A representative heatmap for consistency score evaluation of the screen. Comparisons between Day 10 and 22 post-5-FU time points to week 11 were calculated for each mouse (data in rows) and each miRNA barcode (data in columns). Not detected (N.D.) barcodes are shown in gray. Increased barcodes passing a change threshold are indicated in red, with those below the threshold in blue, and those not changed (neutral) in white.

(B) Barcode intensity decreases for miR-150 were compared in individual recipient mice between Day 10 or Day 22 post-5-FU and Week 11 pre-5-FU time points. A total of 13 mice had a detectable miR-150 barcode signal associated with these time points, with mouse identification (ID) shown at bottom. Day 22 samples for cohort 2 (mice 6–10) did not pass quality control and are not shown (see Experimental Procedures). Solid red line indicates no change. Dashed red lines indicate +0.6 and −0.6 of log2-fold changes that were used as the "change threshold" in (A). The circle (●) indicates that corresponding bar is not shown to the full height.

See also Figure S3 and Table S5.

T lymphoid lineages were overall constitutively inhibited by the expression of miR-150 (Xiao et al., 2007; Lu et al., 2008), reflected by a lower initial GFP^+/GFP^- ratio (Figure S4C). Nevertheless, a ratio drop was also observed post-5-FU (Figure 4A), albeit to a lesser extent than myeloid and platelet lineages. Similar to myeloid cells, the GFP^+/GFP^- ratio of lymphoid cells recovered close to control levels after long duration. The time course of GFP^+/GFP^- ratio normalization suggests that forced expression of miR-150 possibly negatively regulates hematopoietic output from multiple bone marrow progenitor populations, including multipotent progenitors, common myeloid progenitors, and lineage-committed progenitors, but with a lesser effect on long-term stem cells.

miR-150 Knockout Bone Marrow Confers an Accelerated Recovery Response to Hematopoietic Injury

We asked whether loss of miR-150 induces an opposite phenotype as compared to miR-150 gain of function, i.e., accelerating hematopoietic recovery. The germline miR-150 knockout mice were viable and normal in fertility, development, and behavior (Xiao et al., 2007). Further examination of hematopoietic tissues revealed largely normal steady-state hematopoiesis. Peripheral myeloid, lymphoid, and red cell counts of $miR\text{-}150^{-/-}$ mice were indistinguishable from wild-type littermates (Figures 5A and S5B). Similarly, proportions of bone marrow and spleen $Ter119^+$, $Mac1^+$, $CD3^+$, and $B220^+$ cell lineages were similar to controls (Figure S5C). Although peripheral platelet counts and spleen megakaryocyte frequency trended lower in the knockouts, the differences were not statistically significant (Figures 5A and S5D). Note that although changes in specific B cell subsets (Figure S5A), NK, and iNKT cells have been reported in miR-150 knockout mice (Xiao et al., 2007; Bezman et al., 2011; Zheng et al., 2012), changes in these populations were not expected to change the overall peripheral blood cell counts.

To investigate hematopoietic injury response, we conducted competitive recovery experiments, as illustrated in Figure 5B. We genetically labeled the majority of platelets and nucleated blood cells by crossing $miR\text{-}150^{-/-}$ mice with β-actin-GFP mice (Okabe et al., 1997). Bone marrow cells from GFP^+

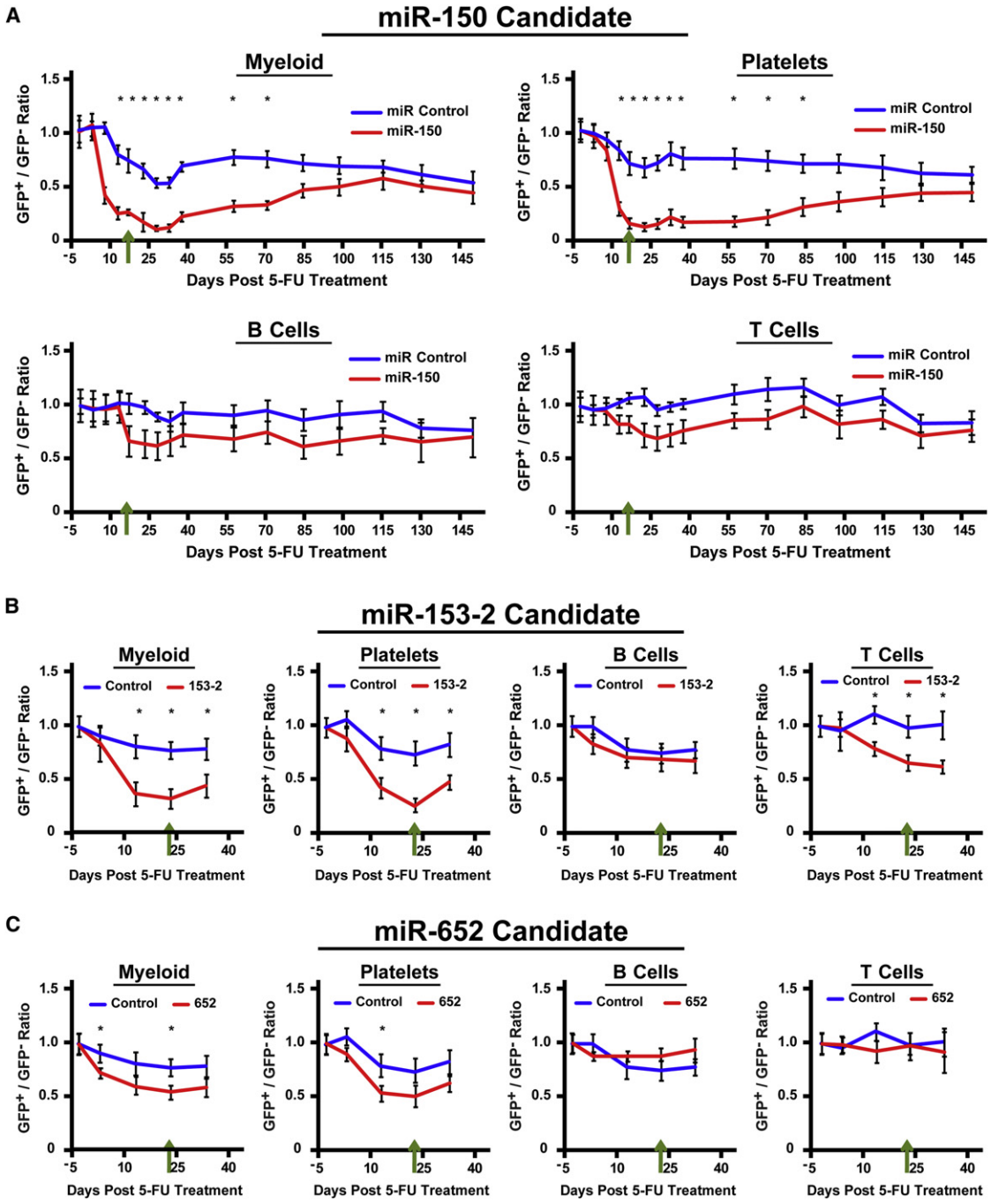

Figure 4. Forced Expression of miR-150 and Other Candidates Impairs Hematopoietic Recovery upon 5-FU Treatment

(A–C) Competitive recovery of transduced cells (GFP^+) compared with nontransduced cells (GFP^-) in mosaic transplantation hosts is shown for $Mac1^+$ myeloid, $B220^+$ B cell, $CD3^+$ T cell lineages, and $CD41^+$ platelets in the peripheral blood. Green arrow indicates the time point of maximal difference among the miR-150 (A), miR-153-2 (B), miR-652 (C), and control cohorts in platelets, myeloid, B cell, and T cell lineages. GFP^+/GFP^- ratios were normalized to that of day −3 before 5-FU treatment. Error bars represent SD (n = 15 for A, n = 4 for B and C). *$p < 0.05$.

See also Figure S4.

miR-$150^{-/-}$ or GFP^+ miR-$150^{+/+}$ mice were mixed 1:1 with GFP^- wild-type bone marrow and transplanted into wild-type recipients. After reestablishment of hematopoietic homeostasis and GFP^+/GFP^- ratio stabilization (Figure S5E), recipient mice were challenged with 5-FU. Examination of peripheral blood GFP^+/GFP^- ratios indicated that miR-$150^{-/-}$ myeloid cells and platelets recovered faster than wild-type controls (Figure 5C). Significant differences of the competitive ratio for platelets between

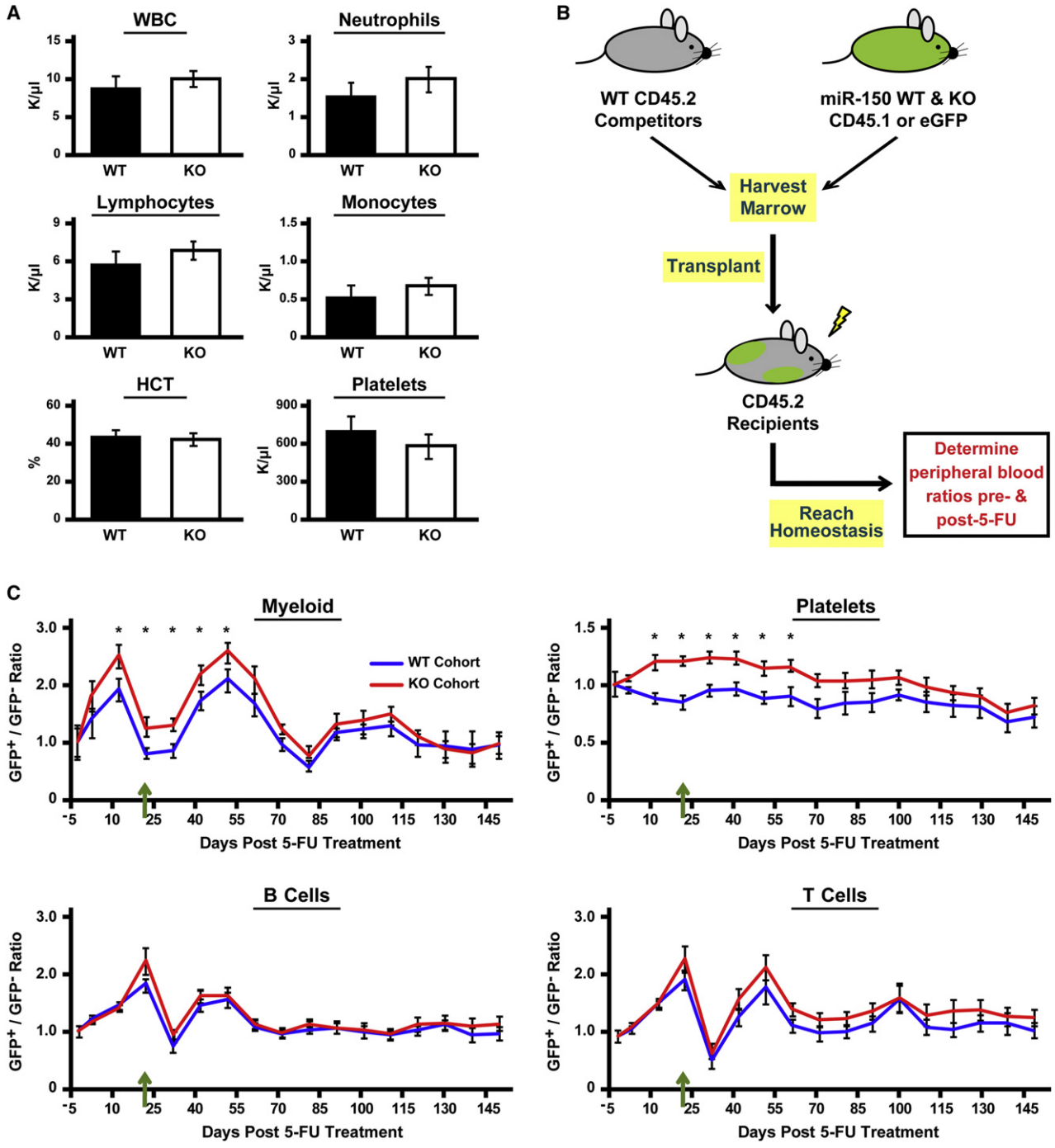

Figure 5. miR-150 Null Bone Marrow Confers Faster Peripheral Recovery upon 5-FU Injury

(A) The homeostatic levels of blood parameters are indistinguishable between wild-type (WT) and miR-150 knockout (KO) littermates. Complete blood counts are shown. WBC, white blood cells; HCT, hematocrit. Error bars indicate SD (n = 12).

(B) A schematic depicting competitive recovery assays comparing wild-type or miR-150 knockout cells with wild-type competitor bone marrow. Transplant recipients were tested for 5-FU injury response after donor bone marrow cells repopulated the recipient hematopoietic system and reached homeostasis. GFP was used to trace miR-150 knockout cells or those from wild-type littermates. CD45.1 and CD45.2-based tracing was used in a parallel experiment (see also Figure S5G). eGFP, enhanced green fluorescent protein.

(C) Competitive recovery of GFP^+ miR-150 knockout cells or that of wild-type controls was compared with wild-type competitors (GFP^-) and measured by peripheral GFP^+/GFP^- ratios. Data were from two independent cohorts and normalized to the ratios 3 days before 5-FU treatment. Error bars represent SD (n = 12). Green arrow indicates the time point with maximal difference between WT and KO cohorts for myeloid cells. *$p < 0.05$.

See also Figure S5.

knockout and control cohorts were observed from day 12, with the maximum increase of 34.5% at 22 days post-5-FU. For myeloid cells, a maximal ratio increase of 50.1% was also observed at day 22. B and T lymphocytes showed only minor ratio alterations, similar to the aforementioned forced expression model.

Unexpectedly, the GFP^+/GFP^- ratios of myeloid and lymphoid cells (but not platelets) showed a time-dependent fluctuation, even in the wild-type control cohort, which may be partially due to incomplete GFP labeling of hematopoietic cells in β-actin-GFP mice (~69% GFP^+ in peripheral $Mac1^+$ cells; ~72% in B220+ cells; ~75% in $CD3^+$ cells; ~81% in platelets). To eliminate the possibility that the differences we observed were due to artifacts of GFP^+/GFP^- ratio fluctuation, we performed competitive recovery experiments using different isoforms of CD45. Similar to the GFP model, bone marrow from $CD45.1^+$ littermates of miR-$150^{-/-}$ or miR-$150^{+/+}$ mice was mixed 1:1 with $CD45.2^+$ wild-type bone marrow cells and transplanted into lethally irradiated $CD45.2^+$ recipients (Figure 5B). 5-FU was administered following recovery from transplantation and $CD45.1^+/CD45.2^+$ ratio stabilization (Figure S5F). Consistent with the GFP model, the myeloid lineage showed faster recovery in the knockout cohort, whereas B and T lymphocytes were largely similar to controls (Figure S5G). Because CD45 is not expressed on platelets, platelet ratios could not be assessed. Taken together, the aforementioned experiments established that loss of miR-150 accelerated the recovery of myeloid and platelet lineages after injury.

Expression of miR-150 Impairs Bone Marrow Clonogenic Potential upon 5-FU Treatment

To further elucidate how miR-150 inhibits hematopoietic recovery, we reasoned that forced expression of miR-150 could impair the function of multiple bone marrow progenitors upon 5-FU administration. This hypothesis is consistent with our observation in Figure 4A, in which the ratio of miR-150-transduced to -nontransduced cells in the peripheral blood was sharply decreased for several weeks and then gradually recovered after an extended period of time. To test this, we generated bone marrow transplant recipients expressing miR-150 or the vector control. After peripheral GFP^+/GFP^- ratios stabilized, we isolated GFP^+ (transduced) and GFP^- (nontransduced) bone marrow populations from the same recipient mouse and tested their clonogenic potential in vitro. The GFP^+ and GFP^- cells from both miR-150 and control vector recipients gave rise to similar frequencies of myeloid colonies (Figure 6A), indicating that expression of miR-150 did not adversely affect colony formation under homeostatic conditions. In contrast, for bone marrow cells harvested 6 days after 5-FU administration, GFP^+ cells from miR-150 recipients showed an ~2.9-fold decrease in myeloid clonogenic potential, whereas GFP^- cells from the same recipient produced similar frequencies of colonies compared to control vector recipients (Figure 6A). Pre-B cell colonies were less severely affected by miR-150 (Table S4). Upon closer examination, this decrease in myeloid colony formation of miR-150-expressing cells impacted all types of colonies, including erythroid, granulocytic/monocytic, and the more primitive GEMM colonies (Table S4), supporting the notion that multiple types of hematopoietic progenitors were compromised.

We then examined the miR-150 knockout model. Under steady-state hematopoiesis, no difference in myeloid colony number was observed between knockout and wild-type mice. In contrast, when we examined bone marrow after 5-FU treatment, miR-150 knockout cells generated a significant increase in the number of myeloid colonies compared to controls (Figure 6B; Table S4). These data indicate that miR-150 inhibits bone marrow colony formation upon 5-FU-induced injury.

This colony inhibition effect could be due to miR-150 inhibiting hematopoietic progenitor function during stressed hematopoiesis or sensitizing progenitors to 5-FU-induced cell death, or both. We tested the first possibility using a postirradiation hematopoietic recovery model. Wild-type bone marrow cells were transduced with miR-150 or vector control, sorted for GFP^+-transduced cells, and transplanted into irradiated recipients. Ten days after transplantation, miR-150 expression resulted in significantly reduced spleen colony formation (Figure 6C), which is an in vivo measure of hematopoietic progenitor activity (Till and McCulloch, 1961). Importantly, because only the transplant hosts were irradiated but not the donor cells, this experiment measured postinjury responses rather than injury itself. Thus, we conclude that miR-150 can inhibit hematopoietic progenitor function during states of stress or injury.

To investigate whether miR-150 sensitizes bone marrow cells to 5-FU-mediated apoptosis, we first transduced wild-type HSPCs (Lin^-Sca^+ Kit^+) with mir-150 or control vector. Cultured HSPCs were then treated with 5-FU in vitro and monitored for apoptosis by flow analysis of the $AnnexinV^+7AAD^-$ population in transduced (GFP^+) and untransduced (GFP^-) fractions. Compared to controls, miR-150-transduced cells showed higher basal apoptosis, which was further elevated upon 5-FU treatment (Figures 6D and S6A), indicating that miR-150 can sensitize HSPCs to apoptosis in vitro. However, we did not observe changes in apoptosis in vivo using the miR-150 overexpression model described above (Figures 6E and S6B), at 6 days post-5-FU when apoptosis was prevalent (data not shown). These data suggest that the inhibitory effect of miR-150 on bone marrow progenitors may also be due to enhanced apoptotic sensitivity toward injury. Taken together, the data above show that forced expression of miR-150 suppressed the bone marrow clonogenic potential after 5-FU administration.

Heterozygous Loss of the miR-150 Target *c-myb* Partially Phenocopies miR-150 Overexpression

To understand the molecular mechanism by which miR-150 inhibits hematopoietic recovery, we focused on the conserved miR-150 target *c-myb* (Xiao et al., 2007; Lu et al., 2008; Barroga et al., 2008). We asked whether heterozygous loss of *c-myb* could phenocopy miR-150 overexpression, i.e., having a hematopoietic-autonomous effect to suppress hematopoietic output in response to 5-FU-induced injury. We examined a conditional heterozygous *c-myb* model because germline knockout of *c-myb* is embryonic lethal (Mucenski et al., 1991), and conditional homozygous knockout of *c-myb* in the hematopoietic system quickly depletes hematopoietic stem cells (Lieu and Reddy, 2009). In addition, because miRNAs do not completely

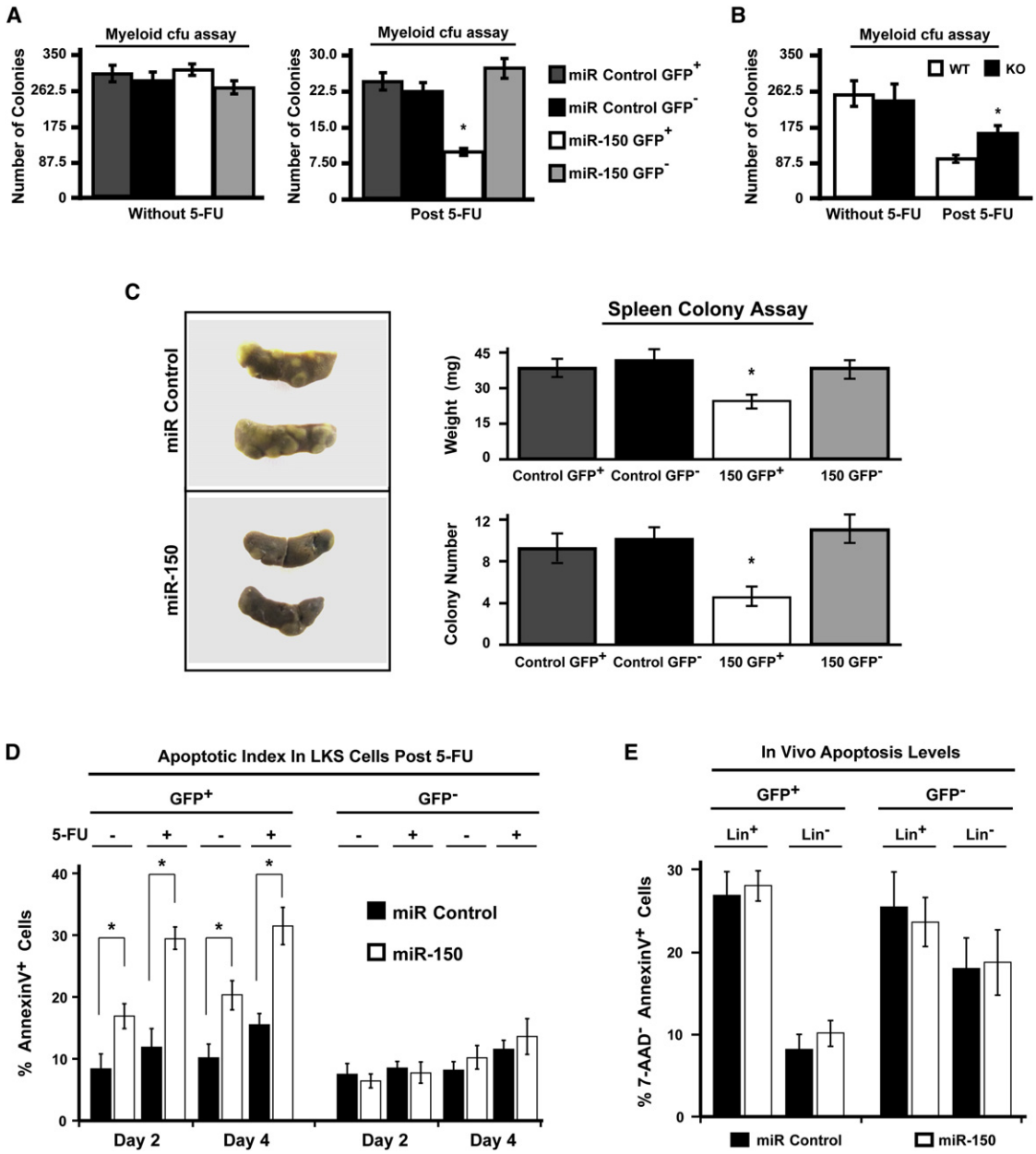

Figure 6. Forced Expression of miR-150 Inhibits Hematopoietic Progenitor Activity upon 5-FU-Induced or Irradiation Injury

(A) Bone marrow cells transduced with miR-150 or a control vector (GFP^+), and those not transduced (GFP^-), were sorted from transplant recipients and were subjected to colony formation assays. Both mice without 5-FU treatment and 6 days post-5-FU were analyzed. Results were from three pairs of miR-150 and control recipients. *$p < 0.05$.

(B) Bone marrow clonogenic potential from wild-type and miR-150 knockout mice was similarly assayed with or without 5-FU treatment ($n = 4$). *$p < 0.05$.

(C) Spleen colony formation potential in miR-150 or control transplant recipients. Wild-type bone marrow was transduced with miR-150 or control vector. GFP^+ cells were sorted, and 1.5×10^4 cells were injected into irradiated recipients. Ten days post transplantation, the number of spleen nodules was counted, and spleen weight was also determined. Images are representative of spleen morphology for each cohort ($n = 4$). *$p < 0.05$. All figure error bars depict the SD.

(D) $Lin^-Kit^+Sca^+$ HSPCs were transduced with miR-150 or a control vector, treated in vitro with or without 5-FU, and assayed at indicated days. $AnnexinV^+$ cells were analyzed after gating on $7AAD^-$ population for both transduced (GFP^+) and untransduced (GFP^-) cells in the same culture. Error bars represent SD ($n = 3$). *$p < 0.05$.

(E) Bone marrow cells from miR-150 or control vector recipients were analyzed for apoptosis by examining the $AnnexinV^+$ $7AAD^-$ population in both Lin^- and Lin^+ populations, 6 days after 5-FU treatment in vivo. Error bars represent SD ($n = 3$).

See also Figure S6 and Table S4.

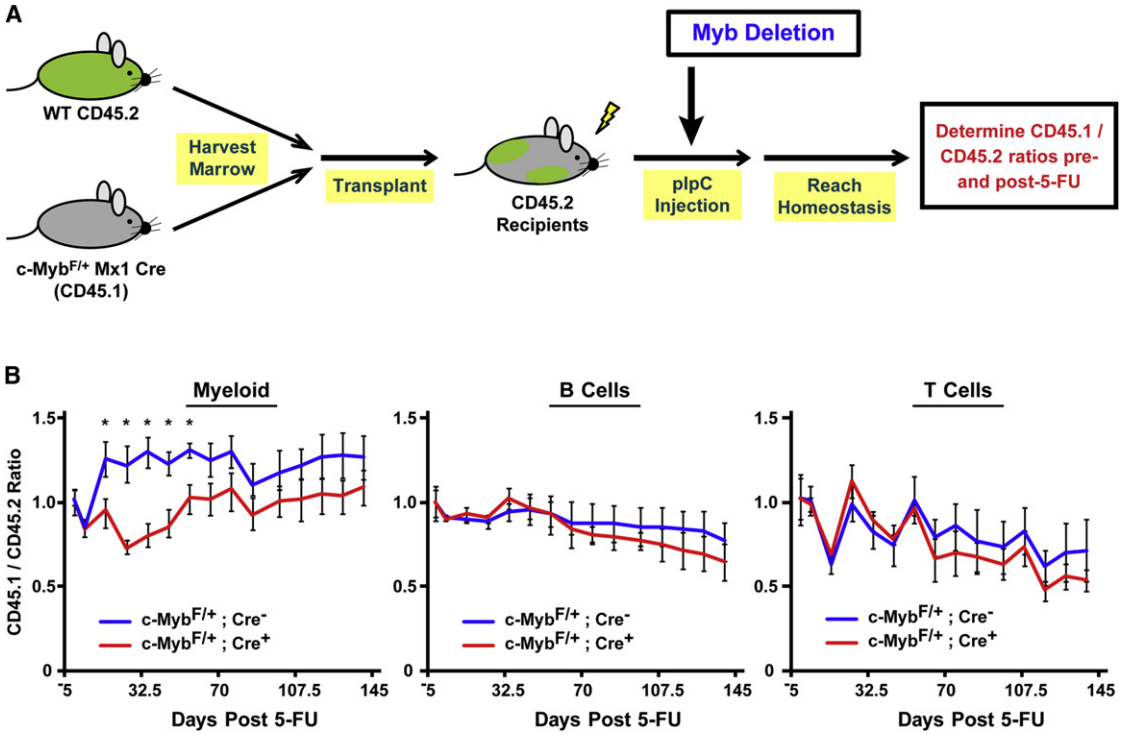

Figure 7. Heterozygous Loss of *c-myb* Partially Phenocopies miR-150-Forced Expression

(A) Schematic of competitive recovery of *c-myb* heterozygous knockout cells. CD45.1/.2$^+$ *Myb*$^{F/+}$Mx1Cre$^+$ bone marrow cells or *Myb*$^{F/+}$Mx1Cre$^-$ cells were cotransplanted with CD45.2$^+$ wild-type cells. After mice recovered from pIpC-induced deletion of *c-myb*, mice were challenged with 5-FU, and competitive recovery was measured in peripheral blood.

(B) The ratios of the test cells (CD45.1/.2) to competitor cells (CD45.2) were measured in peripheral blood before and after 5-FU treatment. The 45.1/45.2 ratios were normalized to the day −3 time point. Error bars represent SD (n = 4). *p < 0.05.

See also Figure S7.

suppress the expression of their target gene(s), heterozygous loss of the target better mimics miRNA action.

Competitive recovery experiments were performed to assay the role of *c-myb* (Figure 7A). CD45.1$^+$/CD45.2$^+$ bone marrow cells from Mx1-Cre$^+$;*Myb*$^{fl/+}$ mice or Mx1-Cre$^-$;*Myb*$^{fl/+}$ mice were mixed 1:1 with CD45.2$^+$ wild-type bone marrow cells and transplanted into CD45.2$^+$ recipients. All recipient mice, regardless of the status of the Mx1-Cre allele, were injected with pIpC, a standard treatment to induce Mx1-Cre expression in the hematopoietic system. After the excision of *c-myb* was confirmed in the Cre$^+$;*Myb*$^{fl/+}$ recipients (Figure S7A) and blood parameters stabilized (Figures S7B and S7C), recipient mice were treated with 5-FU, and the ratio between CD45.1$^+$ cells and competitor CD45.2$^+$ cells was quantified. Note that we waited 35 days between the pIpC and 5-FU treatments to avoid an effect on stem cell activation (Essers et al., 2009). As expected, nonexcisable Mx1-Cre$^-$;*Myb*$^{fl/+}$ cells behaved similarly to wild-type competitor cells. In contrast, Mx1-Cre$^+$;*Myb*$^{fl/+}$ cells showed slower recovery in the myeloid lineage, but not in lymphoid lineages (Figure 7B). We also crossed the Mx1-Cre$^+$;*Myb*$^{fl/+}$ mice with β-actin-GFP mice to examine platelets. Indeed, heterozygous loss of *c-myb* also decreased the platelet recovery rate (Figure S7E), although the level of inhibition on myeloid and platelet lineages was less compared to miR-150 overexpression (Figure 4A). Also similar to the miR-150 overexpression model, myeloid clonogenesis trended lower after 5-FU treatment in heterozygous *c-myb* knockout cells (Figure S7D; Table S4). Overall, these data demonstrate that heterozygous loss of *c-myb* partially recapitulated the phenotypes associated with the miR-150 gain-of-function model.

DISCUSSION

This study demonstrates the feasibility to perform in vivo miRNA screens in live mice with a barcoded library and the power to uncover regulators of complex physiological processes. The finding through the screen that miR-150 impaired hematopoietic injury response contrasts the miRNA expression-profiling results comparing bone marrow samples with or without 5-FU treatment, which found 92 out of 168 (55%) miRNAs with significant expression changes (Figure S1A). Interestingly, miR-150 was among the 45% of miRNAs that were not significantly changed after 5-FU treatment (Table S1). These results reiterate usual problems associated with gene-profiling studies: that the resulting miRNA changes are often too numerous to study. On the other hand, functionally important genes may be missed with profiling. Even after we identified miR-150, measuring miR-150 expression in Kit$^+$ or other potential bone marrow progenitor

populations did not yield intuitive expression patterns associated with its functional importance: miR-150 expression was higher and *c-myb* lower in post-5-FU samples than those without treatment (Figure S6C). Similarly, the complex nature of our measured hematopoietic injury response, which reflects the clinically relevant rebound of circulating mature cells within the peripheral blood after acute injury, can be challenging to model in vitro. We performed two experiments to measure the effect of forced miR-150 expression in cultured Ficoll-purified bone marrow cells but did not observe any differential competitive expansion/survival disadvantage in the presence of varying amounts of 5-FU (data not shown). We only detected changes in apoptosis when starting with purified HSPCs, suggesting that it would have been difficult to discover the role of miR-150 in hematopoietic injury response in a culture dish without the initial in vivo screen.

The bead-based detection system for genetic barcodes is specific and reproducible for functional screens. Compared to next-generation sequencing, it is inexpensive, flexible to design, and more readily accessible. The inexpensiveness makes it more attractive to run small sample batches, such as those during assay set up, or screens with a medium-sized library. It is likely less sensitive compared to next-generation sequencing and less powerful for large genetic libraries, but our detection rate in mouse (92% of the library at 3 weeks) suggests that sufficient sensitivity of detection can be achieved for libraries of ~100–200 genes in complexity.

The data presented in this study highlight the role of miR-150 in controlling hematopoietic recovery after injury. Although the functional screen was designed to uncover regulatory miRNAs that control short-term peripheral blood recovery after acute injury, which is highly relevant to clinical management of patients receiving chemotherapy, the effects with miR-150 overexpression and knockout studies could be seen within the short-term window of 1–3 weeks and also beyond. The miR-150 overexpression model showed weak but significant lymphoid recovery changes, which was not seen in the miR-150 knockout model. This difference may be due to forcing miR-150 expression in cell types that normally do not express miR-150. Our finding, that miR-150 suppresses multiple types of hematopoietic progenitor activities, including both immature and more mature myeloid progenitors upon 5-FU treatment, provides one explanation for the observed short-term and longer-term effects of miR-150. It is important to note that this progenitor cell effect of miR-150 does not contradict previous knowledge of miR-150 in specific lineage differentiation (Lu et al., 2008; Barroga et al., 2008; Xiao et al., 2007; Bezman et al., 2011; Zheng et al., 2012). For example, even though the forced expression of miR-150 elevates platelet production in comparison to myeloid cells (Figure S4C) under homeostatic conditions as expected, upon hematopoietic recovery from acute injury, miR-150 affected more upstream progenitors that largely masked this platelet production bias.

Mechanistically, we show that hematopoietic-intrinsic heterozygous loss of *c-myb* produced similarly delayed recovery after 5-FU. It is known that *c-myb* regulates proliferation and apoptosis-related genes, such as c-*myc*, cyclins, *KIT*, *Bcl-2*, and *Bcl-X*$_L$ (Ramsay et al., 2003; Ramsay and Gonda, 2008), some of which may mediate *c-myb*'s function in hematopoietic recovery. The delayed recovery in the *c-myb* model was both shorter and weaker than the gain of function of miR-150 and did not affect the lymphoid lineages. We speculate that additional targets may also be involved, or the difference in phenotype may be due to quantitative differences in *c-myb* suppression in the two models.

It is intriguing that loss of miR-150 had mild effects on steady-state hematopoiesis (other than B cell subsets, NK and iNKT cells), yet knockout cells displayed the beneficial effect of accelerated rate of hematopoietic recovery in the peripheral blood. This is somewhat puzzling given that miR-150 is evolutionarily conserved from human to frog, although it is possible that the roles of miR-150 in specialized immune cell production, or anti-cancer effect in lymphoma (Chang et al., 2008), contribute to the pressure for genetic conservation. Nevertheless, our data suggest that an interesting avenue to explore in the future will be to temporarily suppress miR-150 activity for the clinically beneficial outcomes of faster platelet and myeloid cell recovery. Because mice null of miR-150 show largely normal behaviors, it suggests that inhibition of miR-150 may have limited side effects. The recent progress in in vivo delivery of miRNA inhibitors (Stenvang et al., 2012) will, in the future, help to test this concept in a more translational setting.

EXPERIMENTAL PROCEDURES

Mouse Strains and Maintenance

All mouse studies were conducted in accordance with federal guidelines and were approved by the Institutional Animal Care and Use Committee of Yale University. See Extended Experimental Procedures for more details.

Constructing a miRNA Expression Library

Design of the retroviral expression library was carried out based on sequence information present in miRBASE v9.0 (Kozomara and Griffiths-Jones, 2011). Desired miRNA hairpins for the library were identified in the human genome, and their ~200 bp flanking sequences were scanned for the presence of other miRNAs or polyA signals. Specific primers (see Table S1) were designed so that they can uniquely amplify the corresponding miRNA, and through a two-step approach, cloned into the pMIRWAY-GFP vector (Guo et al., 2010; Lu et al., 2008). Retrovirus was produced in 293T cells from a pooled plasmid preparation of the pMIRWAY-miRNA library. See Extended Experimental Procedures for more details.

In Vivo miRNA Screen and Barcode Detection

For the in vivo screen, donor adult bone marrow cells were transduced with pooled miRNA viral library, and murine bone marrow transplantation was performed similar to published procedures (Guo et al., 2010). Starting from 3 weeks posttransplantation, genomic DNA isolates from the peripheral blood samples were prepared for barcode detection by first performing PCR to amplify the miRNA cassette. PCR products were purified using a QIAquick PCR Purification Kit (QIAGEN), and miRNA barcodes were detected using a Luminex bead-based detection system. Acquired median fluorescence intensity values were then used in subsequent data analysis. See Extended Experimental Procedures for more details on transplantation, sample preparation, barcode detection, and signal analysis.

Murine Bone Marrow Transplantation

For single miRNA overexpression studies, murine bone marrow transplantation was performed similar to published procedures (Guo et al., 2010). For the miR-150 and *c-myb* competitive transplant assays, bone marrow was collected from donor animals, mixed at a 1:1 mononuclear cell ratio with CD45.2 wild-type competitor cells, and injected into 9.0 Gy irradiated recipient mice.

For determining the GFP ratios of different peripheral blood lineages, peripheral blood was lysed and stained with the following antibody mixture: Mac-1-PE, B220-APC, and CD3-PE-Cy5 in PBS +2% FBS. For experiments using the 45.1 congenic system, CD45.1-FITC was added to the antibody mixture. To assess GFP ratios in platelets, peripheral blood was stained with CD41-PE in sodium citrate buffer, fixed in 1% PFA, and analyzed on FACSCalibur. See Extended Experimental Procedures for details.

Statistical Analysis

Student's t test was used for p value calculation unless specified otherwise.

ACCESSION NUMBERS

The GEO accession number for the miRNA profiling data is GSE39211.

SUPPLEMENTAL INFORMATION

Supplemental Information includes Extended Experimental Procedures, seven figures, and five tables and can be found with this article online at http://dx.doi.org/10.1016/j.celrep.2012.09.014.

LICENSING INFORMATION

ACKNOWLEDGMENTS

We thank Geoffrey Lyon (Yale Cell Sorter Core Facility) for assistance with FACS and analysis. We thank Stacey Baker and Crew Smith for technical assistance. This work was supported in part by the National Institutes of Health Grants 1R01CA149109 (to J.L.), 5K01DK082982 (to S.G.), and 5T32HL007262-34 (to B.D.A.), and the American Cancer Society Institutional Research Grant #58-012-51 (to J.L.).

Received: April 24, 2012
Revised: August 4, 2012
Accepted: September 12, 2012
Published online: October 18, 2012

REFERENCES

Ali, N., Karlsson, C., Aspling, M., Hu, G., Hacohen, N., Scadden, D.T., and Larsson, J. (2009). Forward RNAi screens in primary human hematopoietic stem/progenitor cells. Blood *113*, 3690–3695.

Baltimore, D., Boldin, M.P., O'Connell, R.M., Rao, D.S., and Taganov, K.D. (2008). MicroRNAs: new regulators of immune cell development and function. Nat. Immunol. *9*, 839–845.

Barroga, C.F., Pham, H., and Kaushansky, K. (2008). Thrombopoietin regulates c-Myb expression by modulating micro RNA 150 expression. Exp. Hematol. *36*, 1585–1592.

Bartel, D.P. (2009). MicroRNAs: target recognition and regulatory functions. Cell *136*, 215–233.

Bezman, N.A., Chakraborty, T., Bender, T., and Lanier, L.L. (2011). miR-150 regulates the development of NK and iNKT cells. J. Exp. Med. *208*, 2717–2731.

Bric, A., Miething, C., Bialucha, C.U., Scuoppo, C., Zender, L., Krasnitz, A., Xuan, Z., Zuber, J., Wigler, M., Hicks, J., et al. (2009). Functional identification of tumor-suppressor genes through an in vivo RNA interference screen in a mouse lymphoma model. Cancer Cell *16*, 324–335.

Chang, T.C., Yu, D., Lee, Y.S., Wentzel, E.A., Arking, D.E., West, K.M., Dang, C.V., Thomas-Tikhonenko, A., and Mendell, J.T. (2008). Widespread microRNA repression by Myc contributes to tumorigenesis. Nat. Genet. *40*, 43–50.

Deneault, E., Cellot, S., Faubert, A., Laverdure, J.P., Fréchette, M., Chagraoui, J., Mayotte, N., Sauvageau, M., Ting, S.B., and Sauvageau, G. (2009). A functional screen to identify novel effectors of hematopoietic stem cell activity. Cell *137*, 369–379.

Essers, M.A., Offner, S., Blanco-Bose, W.E., Waibler, Z., Kalinke, U., Duchosal, M.A., and Trumpp, A. (2009). IFNalpha activates dormant haematopoietic stem cells in vivo. Nature *458*, 904–908.

Garzon, R., and Croce, C.M. (2008). MicroRNAs in normal and malignant hematopoiesis. Curr. Opin. Hematol. *15*, 352–358.

Guo, S., Lu, J., Schlanger, R., Zhang, H., Wang, J.Y., Fox, M.C., Purton, L.E., Fleming, H.H., Cobb, B., Merkenschlager, M., et al. (2010). MicroRNA miR-125a controls hematopoietic stem cell number. Proc. Natl. Acad. Sci. USA *107*, 14229–14234.

Hope, K.J., Cellot, S., Ting, S.B., MacRae, T., Mayotte, N., Iscove, N.N., and Sauvageau, G. (2010). An RNAi screen identifies Msi2 and Prox1 as having opposite roles in the regulation of hematopoietic stem cell activity. Cell Stem Cell *7*, 101–113.

Huang, Q., Gumireddy, K., Schrier, M., le Sage, C., Nagel, R., Nair, S., Egan, D.A., Li, A., Huang, G., Klein-Szanto, A.J., et al. (2008). The microRNAs miR-373 and miR-520c promote tumour invasion and metastasis. Nat. Cell Biol. *10*, 202–210.

Izumiya, M., Okamoto, K., Tsuchiya, N., and Nakagama, H. (2010). Functional screening using a microRNA virus library and microarrays: a new high-throughput assay to identify tumor-suppressive microRNAs. Carcinogenesis *31*, 1354–1359.

Kozomara, A., and Griffiths-Jones, S. (2011). miRBase: integrating microRNA annotation and deep-sequencing data. Nucleic Acids Res. *39*(Database issue), D152–D157.

Landgraf, P., Rusu, M., Sheridan, R., Sewer, A., Iovino, N., Aravin, A., Pfeffer, S., Rice, A., Kamphorst, A.O., Landthaler, M., et al. (2007). A mammalian microRNA expression atlas based on small RNA library sequencing. Cell *129*, 1401–1414.

Lieu, Y.K., and Reddy, E.P. (2009). Conditional c-myb knockout in adult hematopoietic stem cells leads to loss of self-renewal due to impaired proliferation and accelerated differentiation. Proc. Natl. Acad. Sci. USA *106*, 21689–21694.

Longley, D.B., Harkin, D.P., and Johnston, P.G. (2003). 5-fluorouracil: mechanisms of action and clinical strategies. Nat. Rev. Cancer *3*, 330–338.

Lu, J., Guo, S., Ebert, B.L., Zhang, H., Peng, X., Bosco, J., Pretz, J., Schlanger, R., Wang, J.Y., Mak, R.H., et al. (2008). MicroRNA-mediated control of cell fate in megakaryocyte-erythrocyte progenitors. Dev. Cell *14*, 843–853.

Lu, R., Neff, N.F., Quake, S.R., and Weissman, I.L. (2011). Tracking single hematopoietic stem cells in vivo using high-throughput sequencing in conjunction with viral genetic barcoding. Nat. Biotechnol. *29*, 928–933.

Lyman, G.H., Dale, D.C., and Crawford, J. (2003). Incidence and predictors of low dose-intensity in adjuvant breast cancer chemotherapy: a nationwide study of community practices. J. Clin. Oncol. *21*, 4524–4531.

Meacham, C.E., Ho, E.E., Dubrovsky, E., Gertler, F.B., and Hemann, M.T. (2009). In vivo RNAi screening identifies regulators of actin dynamics as key determinants of lymphoma progression. Nat. Genet. *41*, 1133–1137.

Mucenski, M.L., McLain, K., Kier, A.B., Swerdlow, S.H., Schreiner, C.M., Miller, T.A., Pietryga, D.W., Scott, W.J., Jr., and Potter, S.S. (1991). A functional c-myb gene is required for normal murine fetal hepatic hematopoiesis. Cell *65*, 677–689.

Okabe, M., Ikawa, M., Kominami, K., Nakanishi, T., and Nishimune, Y. (1997). 'Green mice' as a source of ubiquitous green cells. FEBS Lett. *407*, 313–319.

Poell, J.B., van Haastert, R.J., Cerisoli, F., Bolijn, A.S., Timmer, L.M., Diosdado-Calvo, B., Meijer, G.A., van Puijenbroek, A.A., Berezikov, E., Schaapveld, R.Q., and Cuppen, E. (2011). Functional microRNA screening using a comprehensive lentiviral human microRNA expression library. BMC Genomics *12*, 546.

Ramsay, R.G., and Gonda, T.J. (2008). MYB function in normal and cancer cells. Nat. Rev. Cancer *8*, 523–534.

Ramsay, R.G., Barton, A.L., and Gonda, T.J. (2003). Targeting c-Myb expression in human disease. Expert Opin. Ther. Targets *7*, 235–248.

Stenvang, J., Petri, A., Lindow, M., Obad, S., and Kauppinen, S. (2012). Inhibition of microRNA function by antimiR oligonucleotides. Silence *3*, 1.

Till, J.E., and McCulloch, E.A. (1961). A direct measurement of the radiation sensitivity of normal mouse bone marrow cells. Radiat. Res. *14*, 213–222.

Voorhoeve, P.M., le Sage, C., Schrier, M., Gillis, A.J.M., Stoop, H., Nagel, R., Liu, Y.-P., van Duijse, J., Drost, J., Griekspoor, A., et al. (2006). A genetic screen implicates miRNA-372 and miRNA-373 as oncogenes in testicular germ cell tumors. Cell *124*, 1169–1181.

Wang, J., Sun, Q., Morita, Y., Jiang, H., Gross, A., Lechel, A., Hildner, K., Guachalla, L.M., Gompf, A., Hartmann, D., et al. (2012). A differentiation checkpoint limits hematopoietic stem cell self-renewal in response to DNA damage. Cell *148*, 1001–1014.

Wang, Y., Probin, V., and Zhou, D. (2006). Cancer therapy-induced residual bone marrow injury—mechanisms of induction and implication for therapy. Curr. Cancer Ther. Rev. *2*, 271–279.

Xiao, C., Calado, D.P., Galler, G., Thai, T.H., Patterson, H.C., Wang, J., Rajewsky, N., Bender, T.P., and Rajewsky, K. (2007). MiR-150 controls B cell differentiation by targeting the transcription factor c-Myb. Cell *131*, 146–159.

Zender, L., Xue, W., Zuber, J., Semighini, C.P., Krasnitz, A., Ma, B., Zender, P., Kubicka, S., Luk, J.M., Schirmacher, P., et al. (2008). An oncogenomics-based in vivo RNAi screen identifies tumor suppressors in liver cancer. Cell *135*, 852–864.

Zheng, Q., Zhou, L., and Mi, Q.S. (2012). MicroRNA miR-150 is involved in Vα14 invariant NKT cell development and function. J. Immunol. *188*, 2118–2126.